

Aerodynamic and structural airfoil shape optimisation via Transfer Learning-enhanced Deep Reinforcement Learning

David Ramos¹, Lucas Lacasa², Eusebio Valero^{1,3}, and Gonzalo Rubio^{1,3}

¹ETSIAE-UPM-School of Aeronautics, Universidad Politécnica de Madrid, Plaza Cardenal Cisneros 3, E-28040 Madrid, Spain

²Institute for Cross-Disciplinary Physics and Complex Systems (IFISC, CSIC-UIB), 07122 Palma de Mallorca (Spain)

³Center for Computational Simulation, Universidad Politécnica de Madrid, Campus de Montegancedo, Boadilla del Monte, 28660 Madrid, Spain

June 15, 2025

Abstract

The main objective of this paper is to introduce a transfer learning-enhanced, multi-objective, deep reinforcement learning (DRL) methodology that is able to optimise the geometry of any airfoil based on concomitant aerodynamic and structural criteria. To showcase the method, we aim to maximise the lift-to-drag ratio C_L/C_D while preserving the structural integrity of the airfoil –as modelled by its maximum thickness– and train the DRL agent using a list of different transfer learning (TL) strategies. The performance of the DRL agent is compared with Particle Swarm Optimisation (PSO), a traditional gradient-free optimisation method. Results indicate that DRL agents are able to perform multi-objective shape optimisation, that the DRL approach outperforms PSO in terms of computational efficiency and shape optimisation performance, and that the TL-enhanced DRL agent achieves performance comparable to the DRL one, while further saving substantial computational resources.

1 Introduction

Airfoil design is key to improving the performance and efficiency of various aerodynamic systems, such as aircraft wings, turbine blades, and wind turbines [1]. Such design often predicated on (i) achieving an optimal balance between two aerodynamic forces –where one aims to maximise the aerodynamic lift and minimise the aerodynamic drag– while (ii) maintaining structural integrity [2]. The aerodynamic balance is often explicitly modelled as the lift-to-drag ratio C_L/C_D , where C_L and C_D are the lift and drag coefficients, and the overall problem is mathematised in a so-called objective function $\mathcal{J}(x)$, where x denotes the set of design variables. Finding proper designs thus requires to find the values x that optimise such objective function. Accordingly, airfoil design reduces to a shape optimisation problem.

The two common strategies for airfoil shape optimisation involve, respectively, using gradient-based or gradient-free methods. The former approach utilise the gradient $\nabla\mathcal{J}(x)$, to find the local directions that maximally increase the objective function and iteratively refines the parameters x accordingly [3, 4]. This approach is computationally efficient –particularly with high-dimensional design spaces–, making it a popular choice in aerodynamics as highlighted by comparative studies [5, 6]. The well-known *adjoint method*, introduced in Fluid Dynamics by the seminal work of Pironneau [7], is one prominent example of a gradient-based technique; requiring a computational effort that scales independently of the number of design variables. This method was subsequently refined by the so-called *discrete adjoint method*, becoming a widely used choice in this field [8, 9]. While gradient-based methods are generally efficient and very popular in aerodynamic shape optimisation, they only have provable local convergence, and thus for non-convex objective functions their performance is sensitive to the initial design point [10] and function continuity [3].

On the other hand, gradient-free methods offer an alternative to complex, nonlinear optimisation problems that often appear in aerodynamic design [3, 11]. Despite their higher computational cost compared

to gradient-based methods, they are more robust at finding global optima and handling challenging objective functions [3, 4]. Popular gradient-free methods deployed in the context of airfoil shape optimisation include Genetic Algorithms (GA) [12] or Particle Swarm Optimisation (PSO) [13–15]. As advanced, these methods are often limited by their computational demands and can be inefficient with very large design spaces [6]. To partially bridge these issues, some recent efforts to improve the computational efficiency of gradient-free methods include, e.g., parallel implementations, which can make GAs viable even for intensive applications such as those in aerospace engineering [16].

Recently, deep reinforcement learning (DRL) [17] has emerged as a promising (gradient-free) tool for shape optimisation [18, 19]. DRL methods have indeed demonstrated remarkable capabilities in various domains, particularly when dealing with complex high-dimensional data [4]. Their impact in fluid dynamics studies and aeronautical applications indeed belongs to a recent yet rapidly expanding research field that encompasses both general-purpose ML-based fluid mechanics [20–22], and their application to several aeronautical problems [23, 24] with clear industrial impact [25].

In the task of airfoil optimisation, a significant drawback of training DRL algorithms lies in the computational cost associated with solving the aerodynamic flow problem around the airfoil for a concrete shape: while the most accurate approach to solve the aerodynamic flow involves computational fluid dynamics (CFD) techniques, its intrinsic high computational cost requires opting for alternative, approximate solvers. For instance, some recent studies employ panel methods such as *XFoil* [18, 19] to approximate the aerodynamic performance of airfoils, while some other studies [26, 27] focus on further reducing optimisation costs by constructing surrogate models instead. Although the latter offers faster training times and smoother reward variations with respect to the agent’s actions –facilitating the learning process–, these approximate models come at the price of a decrease in accuracy.

Interestingly, one significant advantage of recent deep learning methods in optimisation tasks is their potential to enhance their learning efficiency through so-called *Transfer Learning* [28, 29]: the possibility of pre-training a given model on one task and subsequently fine-tuning it for a related but different task. Transfer learning could also be developed in the context of DRL, accelerating the agent’s learning process by reusing elements such as policies or feature representations and effectively reducing the need for extensive exploration, a particularly valuable trait in aerodynamic optimisation. To the best of our knowledge this approach has been seldom explored, with a few encouraging exceptions for missile control surface and airfoils [28, 30].

Additionally, note that most studies on airfoil shape optimisation focus solely on maximising aerodynamic efficiency [18, 19, 26, 28, 31], without explicitly considering important structural constraints [32] related, e.g., to the airfoil’s area or thickness. Accordingly, there is a need to develop shape optimisation frameworks that aim to maximise the aerodynamic efficiency while preserving the structural integrity of the airfoil. This, we argue, can be interpreted as an example of multi-objective optimisation [26].

To bridge these gaps, here we aim to explore the performance of DRL (enhanced with different possible Transfer Learning strategies) as a gradient-free framework for airfoil shape optimisation that considers the concomitant role of aerodynamic efficiency and structural integrity. To that aim, we define a flexible reward function that combines the lift-to-drag ratio of the flow around the airfoil and the airfoil’s maximum thickness. We initially train our DRL agent using *XFoil* –both for aerodynamic and combined aerodynamic/structural shape optimisation– and show that the DRL agent is successful at both tasks. At this point results are compared with the ones obtained with Particle Swarm Optimisation, certifying the advantage of DRL over more traditional gradient-free methods. We then consider a Transfer Learning scenario where the DRL agent is pre-trained using *NeuralFoil* [33], a faster-yet-less-accurate neural network surrogate model of *XFoil* built using domain knowledge. After an initial pre-training phase, we subsequently fine-tune the agent’s performance through transfer learning, incorporating direct training with *XFoil*. We compare four different transfer learning strategies and demonstrate how this combined approach can be successfully implemented, achieving accuracy levels comparable to those obtained through direct DRL training with *XFoil*, but at a reduced computational cost.

The rest of the paper is organised as follows. In Section 2, we introduce the whole methodology, that combines a refined reward function for multi-objective optimisation, and using transfer learning coupled with reinforcement learning for airfoil shape optimisation. In Section 3, we report the results, comparing DRL agents with PSO (both for aerodynamic and aerodynamic/structural shape optimisation), trained with vs without transfer learning. Finally, in Section 4, we conclude.

2 Methodology

2.1 Problem under study in a nutshell

We consider the two-dimensional (2D) optimisation of an airfoil shape under fixed operating conditions. The conditions chosen for the study are an Angle of Attack $\text{AoA} = 2$ degrees, a Mach number $\text{Ma} = 0.5$, and a Reynolds number $\text{Re} = 10^6$. These represent a typical aerodynamic scenario for subsonic flow, allowing us to investigate the optimisation of airfoil shapes under conditions that are common in practical applications. In general terms, we shall consider an airfoil shape to be ‘better’ than another one when the aerodynamic flow around the airfoil shows an enhanced lift-to-drag ratio. Accordingly, the objective function to be maximised is such ratio, which is computed by applying an aerodynamic solver to any given airfoil geometry. In the next sections, we detail our proposed geometric optimisation framework and its specifications. We introduce a Reinforcement Learning paradigm which is enhanced by a Transfer Learning strategy where the agent suitably switches between using a fast, surrogate aerodynamic solver (*NeuralFoil* [33]) to a slightly slower yet more accurate one (*XFoil* [34]) as the method to assess the aerodynamic flow and to compute the agent’s reward. *XFoil* is a classic model –based on a panel method coupled with a viscous boundary layer formulation– designed for subsonic flows that calculates the pressure distribution on the airfoil and subsequently derives the lift and drag characteristics. It is faster than performing full DNS integration, but is still considered as an actual aerodynamic solver. *NeuralFoil* on the other hand –implemented in a Python-based library– is a ML surrogate model that can provide representation of the viscous, compressible airfoil aerodynamics for nearly any airfoil, with control surface deflections, across a 360-degree angle of attack, at any Reynolds number. *NeuralFoil* has been trained with millions of *XFoil* simulations, enabling rapid calculations of aerodynamic characteristics, albeit with a slight trade-off in accuracy. Unlike *XFoil*, *Neuralfoil* avoids non-convergence issues.

2.2 The basic DRL optimisation framework

The initial aim is to develop a DRL framework, where the DRL *agent* is capable of improving the aerodynamic efficiency of a given airfoil, as illustrated in Fig. 1. To that aim, the agent interacts with the *environment* (the airfoil geometry, which produces a certain aerodynamic flow) and its goal is to find a *policy* that ultimately maximises the lift-to-drag ratio (C_L/C_D) of such aerodynamic flow, by adequately performing *actions* that adjust the design variables.

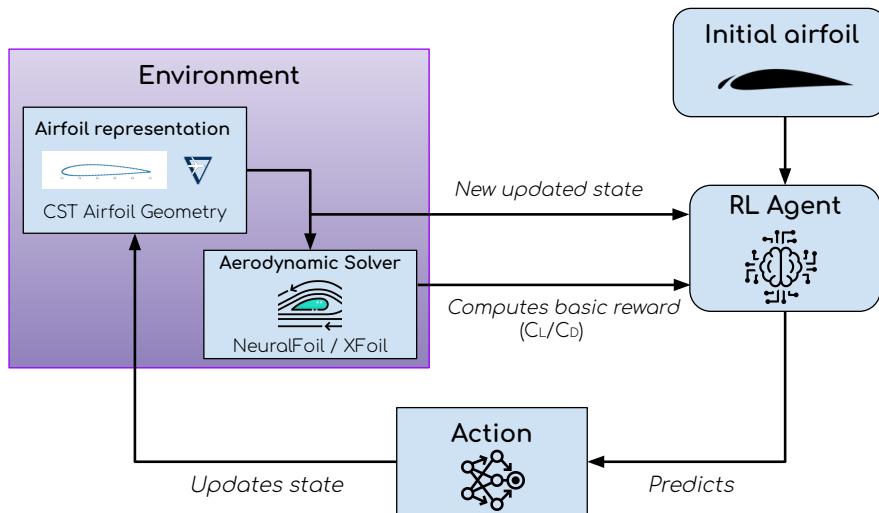


Figure 1: Basic DRL training diagram.

2.2.1 RL specs I: environment, state space and action definition

Environment. The initial stage of the process involves the creation of an *environment* in which the agent can undergo training –see Fig. 1–, and includes (i) choosing an adequate airfoil representation, and (ii) choosing an aerodynamic solver that will compute the aerodynamic properties of the airfoil. Regarding (i), observe that a priori one could simply use the 2D coordinates of the points over the airfoil. However, this choice is delicate as it may lead the agent to explore unusual or even unphysical shapes. A better choice is to use the so-called Class-Shape Transformation (CST) parameters [35], a widely-used technique to parametrise geometries based on the curvature of the shape along the chord. This parameterization indeed generates more realistic shapes and reduces the dimensionality of the design space, allowing for a more efficient optimisation.

The implementation of such environment was done using the Gymnasium Python library [36], a maintained fork of the OpenAI Gym library, which provides a flexible framework for defining and managing RL environments.

State space. The state space spans a total of 18 scalar parameters $\text{STATE} = (s_1, s_2, \dots, s_{18})$, where each parameter is bounded in a concrete range $s_i \in [\text{MIN}(i), \text{MAX}(i)]$. These 18 parameters are extracted from the CST representation, such that eight of them characterise the upper surface, eight of them the lower surface, one for the leading-edge weight, and one for the trailing-edge thickness. Different configuration values of these 18 parameters within their ranges correspond to different airfoil geometries.

Action space and state update. To modify the state of the environment (the airfoil), the agent predicts an action, i.e. a vector $\text{ACTION} = (\text{ACTION}(1), \text{ACTION}(2), \dots, \text{ACTION}(18))$ where $\text{ACTION}(i) \in [-1, 1] \forall i$, as recommended in the documentation of stable baselines¹. This vector is the one performing the change in the parameters that represent the airfoil. Now, to prevent the sequential changes to the airfoil from being too abrupt, we further define a weight vector $\alpha = (\alpha_1, \alpha_2, \dots, \alpha_{18})$, where

$$\alpha_i = \frac{\text{MAX}(i) - \text{MIN}(i)}{\text{EPISODEMAXLENGTH}},$$

where EPISODEMAXLENGTH is a positive integer defined in Sec.2.2.2. Accordingly, updating the state based on the action follows

$$\text{STATE}(i) \leftarrow \text{STATE}(i) + \alpha(i) \cdot \text{ACTION}(i), \quad i = 1, 2, \dots, 18 \quad (1)$$

or in vector form

$$\text{STATE} \leftarrow \text{STATE} + \alpha \odot \text{ACTION}, \quad (2)$$

where \odot is the element-wise multiplication (Hadamard product).

2.2.2 RL specs II: Episode definition

A single step of the DRL agent consists in, given an action, updating the airfoil geometry according to Eq. 2, assessing how this new geometry improves (or not) the aerodynamic efficiency and checking if the termination condition is met. We have decided that this condition will be reached when a maximum number of steps has been completed or if the aerodynamic solver does not converge. The iteration of many steps until the termination condition defines an *episode*, and the number of steps taken is called the episode length.

Here, we initially define the maximum length of an episode as EPISODEMAXLENGTH = 100. Observe that this length needs to strike a balance: if it is too large, the agents will have problems to converge since this would reduce the number of episodes during training and the agents would receive less varied data. Moreover, the number of possible states increases, making the problem more complex. On the other hand, if the length is too short, the values of α in Eq. (2) will be comparatively too large and the airfoil modifications could be too abrupt, further causing instability in the optimisation process.

Once an episode is defined, we need to define how the start of a new episode is carried out. A standard approach is to fix the initial state (to a certain airfoil geometry, e.g. `naca0012`), such that at the beginning of each episode the state of the environment is always reset to the same airfoil. This is, for example, the choice in [18]. Some other studies [19] in turn decide to reset to a different airfoil geometry, the rationale being that in this way the agent is capable of learning to optimise starting from a variety

¹https://stable-baselines3.readthedocs.io/en/master/guide/rl_tips.html#tips-and-tricks-when-creating-a-custom-environment

of shapes, i.e. the learned policy is more universally applicable. Here we chose the latter strategy, so that at the beginning of an episode the environment is chosen at random from a pre-compiled set of 20 *naca* airfoils listed in the Appendix A.1.

2.2.3 RL Specs III: Reward function

Once the episode has been defined, we need to specify the reward function, which estimates the quality of any given action. As a starting point, we consider the lift-to-drag ratio C_L/C_D , where both aerodynamic coefficients are computed from the aerodynamic solver. As previously mentioned, in this work we will use two solvers: *XFoil* and *NeuralFoil*.

In addition to calculating lift and drag, *Neuralfoil* also returns a ‘confidence’ value: a scalar $\kappa \in [0, 1]$ that indicates how confident the surrogate model is after making the lift and drag predictions. In order to penalise weird geometries or geometries whose computed aerodynamic properties have large uncertainty, we will aim to maximise $\kappa \cdot (C_L/C_D)$, i.e. we aim at finding geometries that at the same time are improving the lift-to-drag ratio and keeping the confidence high. However, when using solely $\kappa \cdot (C_L/C_D)$ as reward the agent was not able to converge, that is why after looking [18] the reward was built with differences of the form

$$\kappa_i \frac{C_L}{C_D} \Big|_i - \kappa_{i-1} \frac{C_L}{C_D} \Big|_{i-1}.$$

At this point, we need to include an extra-term in the reward –making the optimisation problem a multi-objective one– to model the effect of preserving the maximum thickness MT of the airfoil, the latter being a structural constraint of the airfoil. The rationale is to find optimal geometries from the point of view of their aerodynamic characteristics that, at the same time, keep constant (as much as possible) the maximum thickness, i.e. $MT_i \approx MT_0$, so that the quotient $x_i := MT_i/MT_0$ remains close to 1. To penalise geometries that take such quotient away from one, we then define a Gaussian regularization

$$\lambda_i = e^{-\sigma(x_i-1)^2}, \quad (3)$$

where σ is an hyperparameter that controls the strength of the nonlinear penalisation (see Fig. 2 for an illustration of how the values of λ penalises geometries with non-conserved maximum thickness, for different values of σ). This Gaussian regularisation is inspired by computational fluid mechanics mesh optimisation methods that minimise error while maintaining low computational cost [37, 38]. Finally, we can define the reward at step i as

$$\mathcal{R}_i = \lambda_i \kappa_i \frac{C_L}{C_D} \Big|_i - \lambda_{i-1} \kappa_{i-1} \frac{C_L}{C_D} \Big|_{i-1}, \quad \mathcal{R}_0 := \kappa_0 \frac{C_L}{C_D} \Big|_0. \quad (4)$$

Note that when we use *XFoil* then κ is not defined, in that case we set $\kappa = 1$ in Eq. 4. Similarly,

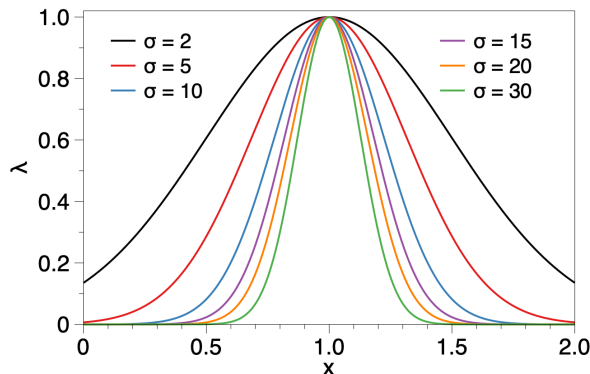


Figure 2: The Gaussian regularization term $\lambda = \exp(-\sigma[x-1]^2)$ as a function of the hyperparameter σ . This term penalises geometries where the airfoil’s maximum thickness deviates from the initial one, as captured by a maximum thickness quotient x that deviates from one.

single-objective optimisation (where maximum thickness is not forced to be preserved) corresponds to the special case $\sigma = 0$.

2.2.4 RL specs IV: the agent

To train an agent with reinforcement learning, one needs to choose the specific DRL algorithm. This choice may depend, among other things, on whether the action space is discrete or continuous. For continuous actions, there are a variety of algorithms, including A2C [39], PPO [40], SAC [41] or TD3 [42]. After a preliminary analysis, we decided to use PPO (Proximal Policy Optimisation), as it shows better convergence properties than A2C and TD3 and SAC have difficulties converging. PPO is a popular policy gradient algorithm that, for instance, is behind the post-training with RLHF of popular Large Language Models, underscoring its versatility. In our implementation, PPO employs neural networks to model the policy and value functions. Specifically, PPO uses an actor-critic framework where the policy network (actor) selects the actions, and the value network (critic) evaluates the expected returns of those actions. Figure 3 shows a schematic of the neural networks comprising PPO. To train the agent, the Python library `Stable Baselines 3` [43] has been used. This is a library that implements different reinforcement learning algorithms and is easy to integrate into `Gymnasium` environments.

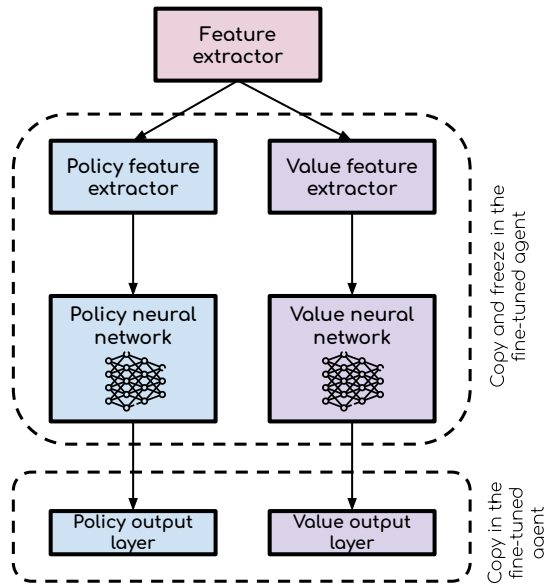


Figure 3: Architecture of the DRL agent that uses Proximal Policy Optimisation. The figure illustrates the transfer learning strategy #3, highlighting the part of the agent’s parameters which are copied and frozen in the fine-tuning phase and the part which is copied and is still trained in during fine-tuning.

2.3 Transfer learning

Finally, we need to explicitly discuss the transfer learning technique. We start by recalling that this is a way of accelerating the training process [28], as it has been observed in RL frameworks that an agent initially trained with a (fast) low-cost model over a substantial number of iterations and subsequently trained with a high-cost model over a limited number of iterations achieves a comparable performance with respect to training solely with a high-cost model over a longer period. Transfer learning thus reduces the overall computational cost and time required for the training process, something particularly welcome in high-cost applications such as aerodynamic shape optimisation. Here, as previously discussed, we use the surrogate model *NeuralFoil* as the low-cost model, and *XFoil* as the more accurate yet more computationally expensive solver. To provide a more effective evaluation of the efficacy of Transfer Learning we use the smallest model available of *Neuralfoil*, which has a clear speed advantage and a clearly lower accuracy compared to *XFoil*.

In practice, we fine-tune the actor-critic neural network utilised by the PPO algorithm. Fine-tuning is a common technique in machine learning where a pre-trained model is adapted to a new task or domain by continuing the training process with different data. Accordingly, here the initial step is to train an agent with the low-cost model. Subsequently, the weights of this agent are transferred to a new agent that is then trained with the high-cost model. Several different approaches have been considered:

- #1 : Share all the parameters of the network and continue with the training.
- #2 : Share all parameters except those of the last layer, both for the action network and the value network, and then continue with the training.
- #3 : Share all the parameters, freeze all of them except those of the last layer of the network, and continue the training.
- #4 : Share all the parameters except those of the last layer of the network, both for the action network and the value network, freeze them, and continue the training.

To clarify, by ‘freezing of weights’ during fine-tuning we mean that they will not be changed. Fig. 3 illustrates how the weight transfer is performed for the specific scenario raised on strategy #3. Finally, note that after pre-training the first agent, an entropy term is added to the PPO loss function, which encourages the new model to explore the state space. This makes it easier for this new agent to move into other areas of the state space. The PPO configurations for each case are described in Appendix B.3.

3 Results

Results cover a variety of analysis of the DRL agents, see Appendices B.1 and B for an in-depth study of the hyperparameter selection and the final configurations of the different PPO hyperparameters. We initially compare the performance and training’s computational efficiency of the DRL agent (trained for the single-objective, aerodynamic optimisation and trained on multi-objective, aerodynamic/structural optimisation) with respect to a traditional gradient-free optimisation methodology, namely Particle Swarm Optimisation (PSO). Then we perform a more detailed analysis of the performance of the DRL agent in the single vs multi-objective scenario. Finally, we assess the performance and efficiency gain when the DRL agent is enhanced with different possible Transfer Learning strategies.

We recall that each episode has at most 100 steps and that training airfoils are sampled randomly at the beginning of each episode from the set of 20 airfoils specified in previous sections. On top of the computing the reward in every step following Eq. 4, we monitor the average episode’s reward each `N_STEPS`, see Appendix B for details. The episode reward is defined simply as the sum of the rewards \mathcal{R}_i of each step i in an episode. The criterion to finish training is based on observing a plateau in this metric.

Once the DRL agent is trained, we evaluate its performance by running a whole episode on the set of airfoils in the *Aerosandbox* [44] Python library, which is essentially a superset of the UIUC Airfoil dataset. This dataset includes a broad variety of airfoils, which allows for a comprehensive evaluation of the agent’s ability to generalise across different shapes and aerodynamic characteristics. In the evaluation, we always use *XFoil* as the method to compute the lift-to-drag ratios, so as to have a fair way of comparing agents. Now, since *XFoil* is known to sometimes have convergence issues, the total number of airfoils evaluated fluctuates a bit between agents.

The evaluation metrics include the best lift-to-drag ratio attained within each episode

$$\mathbf{best} = \max \left\{ \frac{C_L}{C_D} \Big|_i \right\}_{\text{episode}},$$

and the net improvement (in lift-to-drag ratio units) within each episode

$$\mathbf{improvement} = \mathbf{best} - \frac{C_L}{C_D} \Big|_{\text{initial}}.$$

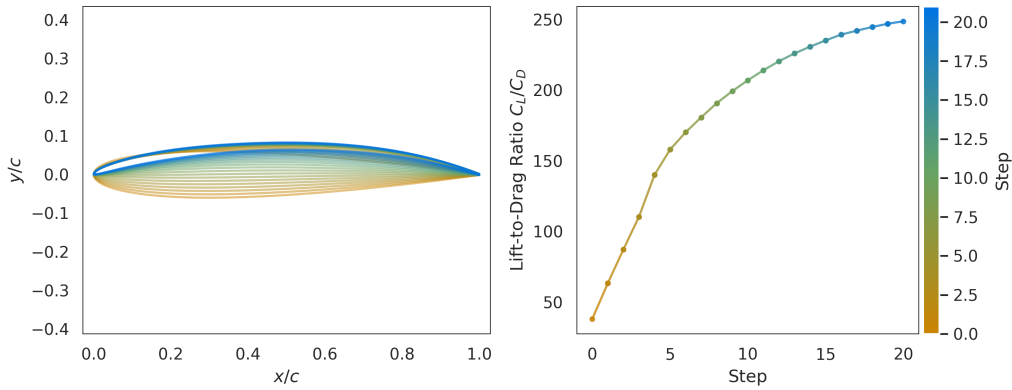
Additionally, in the multi-objective case we monitor the deviation of the airfoil’s maximum thickness with the percentage

$$\Delta_{\text{MT}} = \frac{|\text{MT}_{\text{opt}} - \text{MT}_{\text{ini}}|}{\text{MT}_{\text{ini}}} \cdot 100,$$

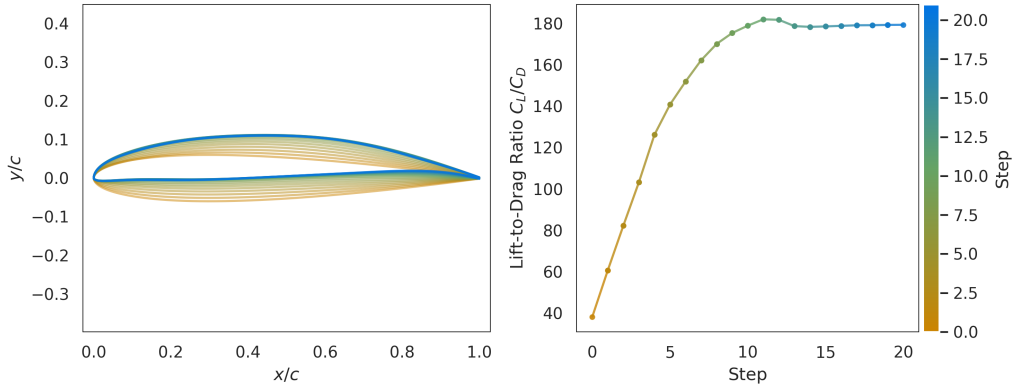
where MT_{ini} and MT_{opt} are the maximum thickness of the initial airfoil and the airfoil with best lift-to-drag ratio, respectively.

3.1 Deep Reinforcement Learning *vs* Particle Swarm Optimisation

This section assesses the proposed DRL methodology and compares it (both in the single and multi-objective versions) with a traditional gradient-free method: Particle Swarm Optimisation (PSO) [45]. PSO is a population-based optimisation algorithm inspired by the social behavior of bird flocks searching for corn. It is widely used due to its simplicity, ability to handle non-differentiable objective functions, and efficiency in exploring high-dimensional search spaces. PSO has been successfully applied in various domains, including image and video analysis applications, engineering design and neural networks, and fluid dynamics optimisation. Furthermore, PSO has proven effective in airfoil optimisation [13–15]. Here, we use *Xoptfoil2* [46] to perform PSO optimisation, since this tool is well designed to compare PSO and DRL as it actually makes calls to *XFoil* underneath. The chosen PSO parameters are the default ones that this library provides. The results obtained using this tool are systematically compared to those given by the DRL agent trained for 81920 steps using *XFoil*. The configuration of *XFoil* used in the training of the DRL agent and the PSO optimiser is detailed in Table 11.



(a) Optimisation of a NACA0012 airfoil by a DRL agent trained on single-objective aerodynamic optimisation.



(b) Optimisation of a NACA0012 airfoil by a DRL agent trained on multi-objective aerodynamic/structural optimisation ($\sigma = 15$).



(c) Left: initial NACA0012 airfoil. Center: single-objective aerodynamic optimisation. Right: multi-objective aerodynamic/structural optimisation ($\sigma = 15$).

Figure 4: Illustration of a DRL policy (20 steps) on NACA0012 trained on aerodynamic and aerodynamic/structural optimisation, respectively.

We start with the single-objective optimisation case, where the DRL agent is trained to solely improve the aerodynamic efficiency of the airfoil. For illustration, the first 20 steps of the DRL policy, as applied to the initial airfoil NACA0012, is shown in Fig. 4a, whereas the airfoil reaching the highest lift-to-drag ratio is depicted in Fig. 4c (center). We clearly see that the DRL agent’s policy is able to substantially and monotonically increase the aerodynamic efficiency of the airfoil.

Now, to initially compare the performance of DRL and PSO optimisation, we select 20 airfoils at random from the UIUC dataset –checking that they represent a wide variety of shapes– and subsequently applied the policies from DRL and PSO. We have made available the whole optimisation trajectory for all 20 airfoils as videos: see here² and here³ for the DRL and PSO trajectories, respectively. The initial and final C_L/C_D results of these trajectories are shown in Table 1. We find that DRL outperforms PSO in most of the cases, certifying the suitability of DRL for airfoil shape optimisation and suggesting its supremacy over PSO.

Then, we tackle the whole UIUC airfoil dataset and proceed to make the full comparison between DRL and PSO. The performance metrics **best** and **improvement** (averaged over the whole set of evaluated airfoils) are depicted in Table 2, certifying the supremacy of DRL over PSO for aerodynamic optimisation.

Airfoil	Initial	PSO single	DRL single	PSO multi	DRL multi
naca0012	38.32	47.72	249.4	45.91	103.6
naca2412	80.53	216.7	257.1	162.2	184.1
s1223	93.69	239.1	204.4	156.2	115.0
fx63143	76.12	86.67	217.4	63.57	102.1
e387	119.9	209.2	224.8	194.9	197.3
naca4412	113.0	223.0	250.7	163.4	141.0
naca63-2a015	54.34	158.8	76.5	117.9	104.8
clarky	107.2	215.1	225.5	164.5	181.7
e174	122.0	218.7	231.3	194.4	197.0
mh113	116.9	247.1	254.9	145.3	169.4
ag25	102.7	250.5	249.8	215.1	215.0
raf48	71.33	201.5	248.4	138.0	159.1
naca23015	43.53	146.0	257.3	86.30	167.7
sc20012	31.69	51.24	201.0	45.19	157.0
goe398	100.5	240.5	257.1	142.6	170.7
n64212	75.90	222.5	261.8	166.4	133.0
ls013	44.53	52.51	231.6	45.61	168.0
dae21	155.1	203.3	258.0	259.8	177.8
vr7	94.59	236.3	253.6	153.0	187.0
naca66-2415	93.72	199.7	240.8	147.5	160.7

Table 1: Comparison of PSO and DRL performance for single and multi-objective aerodynamic/structural optimisation (in terms of the highest C_L/C_D reached in each of the two optimisation paradigms), across a set of different airfoil with different initial C_L/C_D . On average, DRL reaches better aerodynamic efficiency than PSO.

Method	Evaluated Airfoils	Improvement	Best
PSO (single-objective)	1566	105 ± 50	198(76)
DRL (single-objective)	1456	141 ± 48	243(35)

Table 2: Comparison of PSO and DRL evaluation for single-objective aerodynamic optimisation with the whole UIUC airfoil dataset, certifying the supremacy of DRL over PSO for single-objective aerodynamic optimisation. The **Improvement** metric is provided in terms of mean ± one standard deviation (when averaged over the whole UIUC ensemble), whereas the **best** metric is provided in terms of median (IQR), since its distribution is left-skewed.

In a second step, we then focus on the multi-objective case. For illustration, in Fig. 4b we show the performance of a DRL agent’s policy which was trained on multi-objective, aerodynamic/structural

²https://fermingut.github.io/CETACEO_UPM/rl_optim.html

³https://fermingut.github.io/CETACEO_UPM/ps0_optim.html

optimisation with $\sigma = 15$ (see also Fig. 4c (right)). It is clear that the incorporation of the structural regularisation in the reward function has an impact: the lift-to-drag ratio is still increased (albeit reaching smaller values than in the single-objective case), but now the maximum thickness of the shape seems to be maintained.

Interestingly, within *Xoptfoil2* it is possible to define geometrical constraints –such as e.g. a target maximum thickness– and therefore a fair comparison between DRL and PSO within the multi-objective case discussed in Sec. 3.2 is possible too. For illustration, in this comparison we set $\sigma = 15$ (that we will later show to achieve a good balance between aerodynamic optimisation and maximum thickness conservation). A summary of the performance of the 20 previously selected evaluation airfoils can also be seen in Table 1, (videos of DRL trajectories are available for RL⁴ and PSO⁵), whereas summary statistics of the evaluation over all the converged airfoils of the UIUC airfoil dataset are reported in Table 3. While DRL remains clearly superior in terms of optimising aerodynamic efficiency, PSO seems to make a better job at preserving the maximum thickness for $\sigma = 15$.

Method	Evaluated Airfoils	Improvement	Best	Δ_{MT} (%)
PSO (multi-objective)	1566	64 ± 36	150(61)	0.67 ± 2.21
DRL (multi-objective)	1444	89 ± 37	179(46)	11.5 ± 9.4

Table 3: Comparison of of PSO and DRL performance for multi-objective aerodynamic/structural optimisation ($\sigma = 15$) on the whole UIUC airfoil evaluation dataset. Whereas DRL clearly allows to reach higher aerodynamic efficiency, PSO makes a better job at preserving the maximum thickness. Pointwise statistics of the **Improvement** and **best** metrics are provided as in Table 2.

Finally, we provide a comparison of optimisation time per airfoil (averaged over the whole UIUC evaluation set) for DRL and PSO, as performed on an Intel(R) Xeon(R) Gold 6248R CPU @ 3.00GHz+, with one process and one CPU thread. For concreteness, we focus on the single-objective case (where the maximum thickness is not necessarily preserved, e.g. $\sigma = 0$), although note results are qualitatively similar in the multi-objective case. The DRL agent takes about 23 seconds to optimise all 1566 airfoils, i.e. an average of 0.0147 s/airfoil. Comparatively, PSO was notably slower; actually, too slow to directly perform the optimisation in a single core, so MPI was used to accelerate the evaluation (and then the results per process were inferred). The CPU used has 48 cores, 47 used by worker processes plus the one by master process, and with this setup, optimising all the evaluation set took 22 hours and 26 minutes. Assuming linear acceleration, this means $47 \cdot (22 \cdot 3600 + 26 \cdot 60)/1566 = 2424$ seconds on average per airfoil (using a single process). Accordingly, PSO takes about $1.65 \cdot 10^5$ times more time than DRL to optimise each airfoil using a single process. This highlights the drastic efficiency advantage of DRL, making PSO impractically slow by comparison.

3.2 Hyperparameter exploration in the multi-objective case

Here we provide additional insights on the performance of the DRL agent trained on the multi-objective case (i.e. $\sigma > 0$ in Eq. 4). We systematically vary σ –where larger values of σ provide more weight to the structural optimisation over the aerodynamic one), and assess (i) the number of training steps needed to reach training convergence, (ii) the lift-to-drag ratio performance metrics **improvement** and **best** evaluated on all the airfoils present in the Aerosandbox library and (iii) the variation in the maximum thickness, as a function of the regulariser’s hyperparameter σ . Results (for the converged airfoils) are depicted in Table 4. It can be observed that the number of necessary training steps varies (typically increases) with σ . At the same time, results confirm the evidence illustrated in Fig 4 and show that the DRL agent (i) is able to improve the aerodynamic efficiency while (ii) also maintaining the structural integrity of the airfoil –i.e. certifying the multi-objective capability–. Finally, results also certify that forcing the maximum thickness to be preserved comes at the cost of a smaller improvement of the aerodynamic efficiency.

3.3 Enhancing the DRL-based airfoil optimisation with Transfer Learning

To round off, here we compare the training efficiency and evaluate the performance of the trained DRL agent when training is done using a single aerodynamic solver (*XFoil* alone or, for completeness,

⁴https://fermingut.github.io/CETACEO_UPM/rl_optim_preserving_thickness.html

⁵https://fermingut.github.io/CETACEO_UPM/psu_optim_preserving_thickness.html

σ	Improvement	Best	Δ_{MT} (%)	Airfoils Evaluated	Training steps
0	140 \pm 49	241 (37)	64 \pm 22	1982	81920
2	108 \pm 41	201 (49)	22 \pm 16	1965	120832
5	99 \pm 39	190 (52)	21 \pm 18	1960	120832
10	95 \pm 42	190 (53)	15 \pm 10	1909	120832
15	91 \pm 37	180 (46)	12 \pm 11	1952	120832
20	93 \pm 37	186 (45)	12 \pm 10	1933	120832
30	94 \pm 41	186 (57)	8 \pm 11	1938	501760
100	84 \pm 42	176 (59)	5 \pm 5	1922	1001470
1000	54 \pm 35	137 (46)	7 \pm 8	1897	501760

Table 4: Multi-objective agent evaluation with UIUC for different values of σ . Pointwise statistics of the **Improvement** and **best** metrics are provided as in Table 2, and Δ_{MT} statistics over the whole UIUC is provided in terms of mean \pm one standard deviation.

NeuralFoil alone) with respect to the case when the agent is pre-trained with *NeuralFoil* and fine-tuned with *XFoil*. For the sake of exposition, we separate the single-objective ($\sigma = 0$ in Eq. 4) and the multi-objective ($\sigma > 0$) cases.

Single-objective case. Results for all DRL agents in the single-objective case (with and without transfer learning) are summarised in Table 5, reporting (i) the total number of training steps, (ii) the total solver time, (iii) the number of airfoils evaluated, and the metrics (iv) pointwise statistics of **best** and (v) **improvement** over all the airfoils in the evaluation set. Pointwise statistics of **best** reported in the table are given in terms of median (IQR) as the distributions are not Gaussian (Shapiro-Wilk test) and highly skewed, whereas in the case of **improvement** we report mean \pm std as the distributions are fairly more symmetrical. Note that to compute the total solver time we simply multiply the number of training steps by the execution time per call to the particular aerodynamic solver, which according to Neuralfoil’s GitHub amounts to 73 ms for a call to *XFoil* and 4 ms for a call to the smallest version of *NeuralFoil*, which is the one we actually used. Although the total solver time is not equivalent to the total training time, it is nonetheless an objective way of comparing the computational effort of the agent using vs. not using transfer learning. As previously mentioned, the number of airfoils evaluated slightly varies across agents as *XFoil*, used universally for evaluation, sometimes has convergence issues, and we had to discard those airfoils for which *XFoil* did not converge.

DRL Agent	Training steps	Total solver time (s)	Airfoils evaluated	Improvement	Best
Fully trained with XFoil (no transfer learning)	81920	5980	1982	140 \pm 49	241(37)
Pre-training (<i>Neuralfoil</i>)	26312	105	1970	66 \pm 32	154(33)
Transfer Learning (fine-tuning with strategy #3)	10240	748	1983	120 \pm 43	219(29)
Transfer Learning (fine-tuning with strategy #1)	10240	748	1977	136 \pm 44	236(28)

Table 5: Comparison of the training efficiency and performance at evaluation stage (with the UIUC dataset) for three different agents: one trained with *XFoil* and two that make use of transfer learning, pre-trained with *NeuralFoil* and fine-tuned with *XFoil*. To compute the training time we used the per-step execution times from Neuralfoil’s GitHub, that amounts to 73 ms for a call to *XFoil* and 4 ms for a call to *NeuralFoil*. Pointwise statistics of the **Improvement** and **best** metrics are provided as in Table 2. Results indicate that the TL strategy #1 yields a comparable aerodynamic optimisation and is substantially faster to train.

First, out of the four transfer learning strategies depicted in Sec. 2.3, we found that strategy #1 yielded the best improvement of training time, followed by #3. Strategies #2 and #4 did not actually yield any

notable improvement and are thus not reported in the table. This suggests that the information present in the final layers of the neural network is very influential to the agent’s behaviour.

Second, from the table we observe that the number of necessary training steps for the agent solely trained with *Xfoil* (81920) is notably larger than the total number of steps needed for the DRL agents with transfer learning, where the pre-training (*Neuralfoil*) and fine-tuning totally amounts to $26312 + 10240 = 36552$ training steps. The cost of the steps performed with *Neuralfoil* could be considered negligible, so the important aspect here is that the number of steps required with *Xfoil* is reduced by a factor of 8. Additionally, it can be observed that the total number of iterations decreases. This is because the agent converges with fewer iterations when trained with *Neuralfoil*, something that can be attributed to its continuous nature and its lack of non-convergence problems. This is already evidence that transfer learning reduces the computational effort.

Third, not only the number of steps, but also the total solver time during training (5980 seconds vs. $105 + 748 = 853$ seconds) is notably shorter for the agents trained using transfer learning. On this respect, we have also compared the total training time with and without transfer learning. If we define the **Time Reduction (%)** as

$$\text{Time Reduction} = \frac{\text{TL-free training time} - \text{TL-enhanced training time}}{\text{TL-free training time}} \cdot 100, \quad (5)$$

we find **Time Reduction** $\approx 86\%$, reaching higher reductions than in other settings [30].

Fourth, the performance in the evaluation set of the agent trained solely on *Xfoil* seems statistically superior (Mann-Whitney U test $p < 10^{-9}$), but the DRL agent trained with Transfer Learning (strategy #1) shows a very similar performance (paired sign test $p \approx 0.006$, see boxplots of the **best** performance metric in Fig. 5), confirming that transfer learning indeed increases computational efficiency while maintaining good performance.

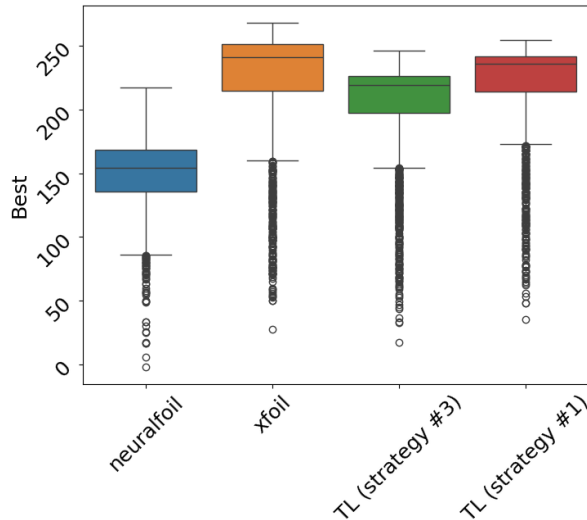


Figure 5: Boxplot of the **best** performance metric in the evaluation set, for all (single-objective) DRL agents, showing whiskers at 1.5 IQR. The DRL agent trained solely on *Xfoil* remains statistically superior (Mann-Whitney U test), but the performance obtained by the DRL agent trained with transfer learning’s strategy #1 is very close.

Finally, in Fig. 6 we scatter plot the best lift-to-drag ratio obtained for each evaluated airfoil as a function of the initial estimate of the airfoil shape for the four DRL agents. These scatter plots show that while there are some specific shapes for which the agent cannot improve the aerodynamic efficiency, in most of the cases all DRL agents can improve it, with varying degrees of performance, which are in good agreement with those previously reported. Interestingly, we find that all airfoils with initial $C_L/C_D > 150$ seem to be greatly improved by the DRL agent trained solely with *Xfoil* and the one trained with the Transfer Learning strategy #1 (see the clear exclusion area in panels (A) and (D)).

Multi-objective case. Results of the DRL agent (with TL) trained on a combined aerodynamic/structural optimisation are depicted in Table 6. Comparing these with the equivalent results without TL reported

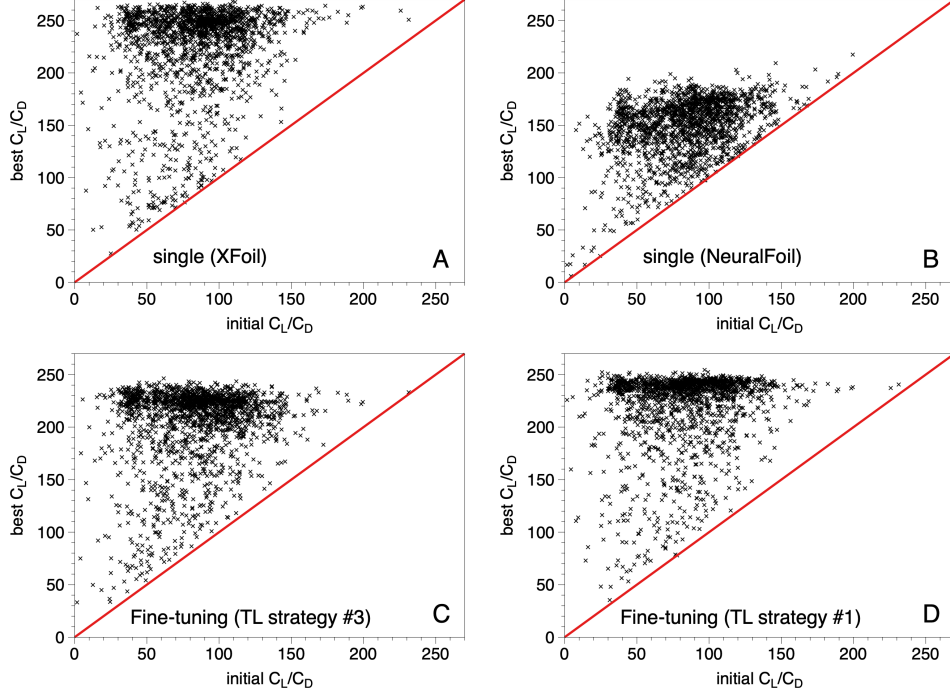


Figure 6: Scatter plots of the metric **best** as a function of the initial lift-to-drag ratio for all airfoils in the evaluation set, as computed from (A) the DRL agent trained with *XFOil*, (B) the pre-training with *NeuralFoil*, (C) the DRL agent trained with transfer learning (strategy #3), and (D) the DRL agent trained with transfer learning (strategy #1), within the single-objective optimisation scenario.

in Table 4, we find that (i) the procedure involving TL substantially reduces the number of training steps as well as the training time, reaching **Time Reduction** as large as 94%; (ii) fixing the structural hyperparameter σ , the improvement in aerodynamic efficiency is only slightly lower for every value of σ (around a 10%) in the TL-enhanced DRL agent than the one without TL, and (iii) the preservation of the maximum thickness is quite similar in both techniques. In summary, TL-enhancement also works in the multi-objective case.

σ	Improvement	Best	Δ MT (%)	Training steps	Airfoils Evaluated	Time Reduction (%)
2	98 ± 37	189 (46)	20 ± 16	25088	1945	78.0
5	92 ± 34	182 (30)	15 ± 15	25088	1961	78.0
10	87 ± 36	178 (38)	13 ± 14	25088	1950	78.0
15	85 ± 36	171 (40)	16 ± 16	35328	1952	69.7
20	82 ± 36	171 (41)	14 ± 13	35328	1958	69.7
30	79 ± 36	171 (46)	14 ± 13	35328	1958	92.6
100	62 ± 35	151 (45)	8 ± 8	50176	1905	94.8
1000	26 ± 22	110 (41)	4 ± 5	50176	1802	89.7

Table 6: Multi-objective, TL-enhanced DRL agent evaluation with the UIUC dataset, for different values of the structural hyperparameter σ . Pointwise statistics of the **Improvement** and **best** and Δ MT are provided like in Table 4. **Time Reduction** is computed with Eq. 5, by comparing the training time spent by the multi-objective DRL agent with and without TL.

4 Conclusions

While traditional airfoil shape optimisation typically considers aerodynamic efficiency, the optimisation can produce airfoils whose structural integrity might be compromised; in other words, there is a need to preserve some structural constraints –such as the airfoil’s maximum thickness– within the optimisation

process. In this paper, we have developed a technique for airfoil shape optimisation –flexible to accommodate single-objective (aerodynamic) or multi-objective (aerodynamic/structural) shape optimisation– that enhances a deep reinforcement learning (DRL) agent with Transfer Learning (TL). Our results indicate that (i) DRL works both for the aerodynamic and aerodynamic/structural shape optimisation problems, (ii) DRL is notably superior to other gradient-free methods such as Particle Swarm Optimisation (PSO) in terms of computational efficiency (being several orders of magnitude faster) and aerodynamic performance, although PSO seem to enforce thickness constraints almost exactly, while DRL does that only approximately, (iii) and the TL-enhancement reduces further training costs with respect to the TL-free case, while approximately maintaining performance (in terms of aerodynamic efficiency and structural preservation).

In summary, our results suggest that DRL stands as an efficient method for airfoil optimisation, both in terms of increasing aerodynamic efficiency and also in the search of geometries that at the same time have enhanced aerodynamic properties and realistically preserve structural constraints. At the same time, the efficiency of this optimisation technique might enable the incorporation of gold standard -yet expensive- aerodynamic solvers, such as CFD-based optimisation, something that also deserves future investigation. Finally, a more general and exciting open problem is to assess whether the benefits of this combined technique also apply in other problems that encompass aerodynamic and structural shape optimisation, e.g. maximisation of lift-to-drag ratio or flow, minimisation of mass, pressure drop, or stress concentration, and maintaining strength or stiffness, and their application to e.g. pipe shapes, car frames, or fillet optimisation to cite a few.

Acknowledgments

The authors acknowledge funding from project TIFON (PLEC2023-010251) funded by MCIN/AEI/10.13039/501100011033, Spain. The authors acknowledge funding from the European Union (project HERFUSE) under GA No 101140567. Views and opinions expressed are however those of the author(s) only and do not necessarily reflect those of the European Union or Clean Aviation Joint Undertaking. Neither the European Union nor Clean Aviation JU can be held responsible for them. LL acknowledges partial financial support from via project MISLAND (PID2020-114324GB-C22) and the Maria de Maeztu Program for units of Excellence (grant CEX2021-001164-M), both funded by MICIU/AEI/10.13039/501100011033, and funding from the European Commission Chips Joint Undertaking project No. 101194363 (NEHIL). GR acknowledges partial financial support received by the Grant DeepCFD (Project No. PID2022-137899OB-I00) funded by MICIU/AEI/10.13039/501100011033 and by ERDF, EU. Finally, all authors gratefully acknowledge the Universidad Politécnica de Madrid (www.upm.es) for providing computing resources on Magerit Supercomputer.

References

- [1] Frank K. Lu. *Airfoil Geometries in Various Flight Vehicles*, chapter Airfoil Geometries. Embry-Riddle Aeronautical University Press, 2022. Accessed: March 06, 2025.
- [2] X. He, N. Qin, and G. Zhu. Balancing design lift and structural stiffness in airfoils. *Journal of Physics: Conference Series*, 524(1):012017, 2014.
- [3] S.N. Skinner and H. Zare-Behtash. State-of-the-art in aerodynamic shape optimisation methods. *Applied Soft Computing*, 62:933–962, 2018.
- [4] P. Garnier et al. A review on deep reinforcement learning for fluid mechanics. *arXiv preprint arXiv:1908.04127*, 2019.
- [5] Marc Secanell and Afzal Suleman. Numerical evaluation of optimization algorithms for low-reynolds-number aerodynamic shape optimization. *AIAA Journal*, 43:2262–2267, 2005.
- [6] Z.; Lyu, Z.; Xu and J.R.R.A. Martins. Benchmarking optimization algorithms for wing aerodynamic design optimization. In *8th International Conference on Computational Fluid Dynamics*. Citeseer, 2014.
- [7] O. Pironneau. On optimum design in fluid mechanics. *Journal of Fluid Mechanics*, 64:97–110, 1974.

- [8] P. D.; Frank and G. R. Shubin. A comparison of optimization-based approaches for a model computational aerodynamics design problem. *Journal of Computational Physics*, 98:74–89, 1992.
- [9] Antony Jameson, Luigi Martinelli, and Neil Pierce. Optimum aerodynamic design using the navier-stokes equations. *Theoretical and Computational Fluid Dynamics*, 10(3):213–237, 1998.
- [10] L. Jichao, D. Xiaosong, and J. R.R.A.Martins. Low-reynolds-number airfoil design optimization using deep-learning-based tailored airfoil modes. *Aerospace Science and Technology*, 121:567, 2022.
- [11] Jonathan Viquerat, Jean Rabault, Alexander Kuhnle, Hassan Ghraieb, Aurélien Larcher, and Elie Hachem. Direct shape optimization through deep reinforcement learning. *Journal of Computational Physics*, 428:110080, 2021.
- [12] Nadia Bizzarrini, Francesco Grasso, Domenico P Coiro, et al. Genetic algorithms in wind turbine airfoil design. *EWEA, EWEC2011, Bruxelles, Belgium*, 14, 2011.
- [13] Y.-Y. Wang, B.-Q. Zhang, and Y.-C. Chen. Robust airfoil optimization based on improved particle swarm optimization method. *Applied Mathematics and Mechanics*, 32:1245–1254, 2011.
- [14] P. Fourie and A.A. Groenwold. The particle swarm optimization algorithm in size and shape optimization. *Structural and Multidisciplinary Optimization*, 23:259–267, 2002.
- [15] A. Nejat, P. Mirzabeygi, and M.S. Panahi. Airfoil shape optimization using improved multiobjective territorial particle swarm algorithm with the objective of improving stall characteristics. *Structural and Multidisciplinary Optimization*, 49:953–967, 2014.
- [16] J. Wang, J. Periaux, and M. Sefrioui. Parallel evolutionary algorithms for optimization problems in aerospace engineering. *Journal of Computational and Applied Mathematics*, 149:155–169, 2002.
- [17] Kai Arulkumaran, Marc Peter Deisenroth, Miles Brundage, and Anil Anthony Bharath. Deep reinforcement learning: A brief survey. *IEEE Signal Processing Magazine*, 34(6):26–38, 2017.
- [18] Thomas P Dussauge, Woong Je Sung, Olivia J Pinon Fischer, and Dimitri N Mavris. A reinforcement learning approach to airfoil shape optimization. *Scientific Reports*, 13(1):9753, 2023.
- [19] Jinhua Lou, Rongqian Chen, Jiaqi Liu, Yue Bao, Yancheng You, and Zhengwu Chen. Aerodynamic optimization of airfoil based on deep reinforcement learning. *Physics of Fluids*, 35(3):037128, March 2023.
- [20] S. L. Brunton, B. R. Noack, and P. Koumoutsakos. Machine learning for fluid mechanics. *Annual Review of Fluid Mechanics*, 52:477–508, 2020.
- [21] R. Vinuesa, S. L. Brunton, and B. J. McKeon. The transformative potential of machine learning for experiments in fluid mechanics. *Nature Reviews Physics*, 5(9):536–545, 2023.
- [22] R. Vinuesa and S. L. Brunton. Enhancing computational fluid dynamics with machine learning. *Nature Computational Science*, 2(6):358–366, 2022.
- [23] S. Le Clainche, E. Ferrer, S. Gibson, E. Cross, A. Parente, and R. Vinuesa. Improving aircraft performance using machine learning: a review. *Aerospace Science and Technology*, 108354, 2023.
- [24] Steven L Brunton, J Nathan Kutz, Krithika Manohar, Aleksandr Y Aravkin, Kristi Morgansen, Jennifer Klemisch, Nicholas Goebel, James Buttrick, Jeffrey Poskin, Adriana W Blom-Schieber, et al. Data-driven aerospace engineering: reframing the industry with machine learning. *Aiaa Journal*, 59(8):2820–2847, 2021.
- [25] Lucas Lacasa, Abel Pardo, Pablo Arbelo, Miguel Sánchez, Noelia Bascones, Pablo Yeste, Alejandro Martínez-Cava, Gonzalo Rubio, Ignacio Gómez, Eusebio Valero, et al. Towards certification: A complete statistical validation pipeline for supervised learning in industry. *Expert Systems with Applications*, page 127169, 2025.
- [26] Ziyang Liu, Miao Zhang, Di Sun, Li Li, and Gang Chen. A deep reinforcement learning optimization framework for supercritical airfoil aerodynamic shape design. *Structural and Multidisciplinary Optimization*, 67(3):34, March 2024.

- [27] Jiaqi Liu, Rongqian Chen, Jinhua Lou, Hao Wu, Yancheng You, and Zhengwu Chen. Airfoils optimization based on deep reinforcement learning to improve the aerodynamic performance of rotors. *Aerospace Science and Technology*, 143:108737, December 2023.
- [28] Xinghui Yan, Jihong Zhu, Minchi Kuang, and Xiangyang Wang. Aerodynamic shape optimization using a novel optimizer based on machine learning techniques. *Aerospace Science and Technology*, 86:826–835, 2019.
- [29] T. Noda, K. Okabayashi, S. Kimura, S. Takeuchi, and T. Kajishima. Optimization of configuration of corrugated airfoil using deep reinforcement learning and transfer learning. *AIP Advances*, 13(3):035328, 03 2023.
- [30] Sahil Bhola, Suraj Pawar, Prasanna Balaprakash, and Romit Maulik. Multi-fidelity reinforcement learning framework for shape optimization. *Journal of Computational Physics*, 482:112018, 2023.
- [31] Ying Yuan Liu, Jian Xiong Shen, Ping Ping Yang, and Xin Wen Yang. A cnn-pinn-drl driven method for shape optimization of airfoils. *Engineering Applications of Computational Fluid Mechanics*, 19(1):2445144, 2025.
- [32] Howard P Buckley, Beckett Y Zhou, and David W Zingg. Airfoil optimization using practical aerodynamic design requirements. *Journal of Aircraft*, 47(5):1707–1719, 2010.
- [33] Peter Sharpe and R John Hansman. Neurofoil: An airfoil aerodynamics analysis tool using physics-informed machine learning. *arXiv preprint arXiv:2503.16323*, 2025.
- [34] Mark Drela. Xfoil: An analysis and design system for low reynolds number airfoils. In *Low Reynolds Number Aerodynamics: Proceedings of the Conference Notre Dame, Indiana, USA, 5–7 June 1989*, pages 1–12. Springer, 1989.
- [35] Brenda M Kulfan. Universal parametric geometry representation method. *Journal of aircraft*, 45(1):142–158, 2008.
- [36] Mark Towers, Ariel Kwiatkowski, Jordan Terry, John U Balis, Gianluca De Cola, Tristan Deleu, Manuel Goulão, Andreas Kallinteris, Markus Krimmel, Arjun KG, et al. Gymnasium: A standard interface for reinforcement learning environments. *arXiv preprint arXiv:2407.17032*, 2024.
- [37] David Huergo, Gonzalo Rubio, and Esteban Ferrer. A reinforcement learning strategy for p-adaptation in high order solvers. *Results in Engineering*, 21:101693, 2024.
- [38] David Huergo, Martín de Frutos, Eduardo Jané, Oscar A Marino, Gonzalo Rubio, and Esteban Ferrer. Reinforcement learning for anisotropic p-adaptation and error estimation in high-order solvers. *arXiv preprint arXiv:2407.19000*, 2024.
- [39] Volodymyr Mnih, Adria Puigdomenech Badia, Mehdi Mirza, Alex Graves, Timothy Lillicrap, Tim Harley, David Silver, and Koray Kavukcuoglu. Asynchronous methods for deep reinforcement learning. In *International conference on machine learning*, pages 1928–1937. Pmlr, 2016.
- [40] John Schulman, Filip Wolski, Prafulla Dhariwal, Alec Radford, and Oleg Klimov. Proximal policy optimization algorithms, 2017.
- [41] Tuomas Haarnoja, Aurick Zhou, Pieter Abbeel, and Sergey Levine. Soft actor-critic: Off-policy maximum entropy deep reinforcement learning with a stochastic actor. In *International conference on machine learning*, pages 1861–1870. Pmlr, 2018.
- [42] Scott Fujimoto, Herke Hoof, and David Meger. Addressing function approximation error in actor-critic methods. In *International conference on machine learning*, pages 1587–1596. PMLR, 2018.
- [43] Antonin Raffin, Ashley Hill, Adam Gleave, Anssi Kanervisto, Maximilian Ernestus, and Noah Dormann. Stable-baselines3: Reliable reinforcement learning implementations. *Journal of Machine Learning Research*, 22(268):1–8, 2021.
- [44] Peter D. Sharpe. Aerosandbox: A differentiable framework for aircraft design optimization. Master’s thesis, Massachusetts Institute of Technology, 2021. Available at <https://dspace.mit.edu/handle/1721.1/140023>.

- [45] James Kennedy and Russell Eberhart. Particle swarm optimization. In *Proceedings of ICNN'95-international conference on neural networks*, volume 4, pages 1942–1948. iee, 1995.
- [46] Daniel Prosser Jochen Guenzel. Xoptfoil2: An optimization tool for airfoil design. <https://github.com/jxjo/Xoptfoil2>, 2025. Accessed: 2025-01-15.

A RL environment configuration

This section shows the configuration used for the environments.

A.1 CST parameters

Parameter	Lower bound	Upper bound
Upper surface	8 x [-1.5]	8 x [1.25]
Lower surface	8 x [-0.75]	8 x [1.5]
Trailing-edge thickness	0.0005	0.01
Leading-edge weight	-0.05	0.775

Table 7: CST bounds for the environments

The initial airfoil for an episode is selected from this list of 20 NACA airfoils: naca0006, naca0009, naca0012, naca0015, naca0018, naca1408, naca1410, naca1412, naca2412, naca2415, naca4412, naca4415, naca4420, naca6412, naca6415, naca7421, naca8409, naca8412, naca8415, naca9421

B PPO hyperparameters

If a parameter is not included in a table, the default value given by Stable Baselines 3 will be used.

B.1 Improvement of training efficiency

Sample inefficiency is a common problem for many reinforcement learning algorithms, which means that to learn, the agent needs to see too many simulations. For problems like this, where the simulations are expensive, this could be an issue. To reduce the number of simulations needed and thus the computational cost for the training process, the hyperparameters of PPO have been tuned following this goal. After many trainings, it has been observed that the most relevant parameter in terms of the number of steps needed to train an agent is the discount factor, γ , and the second one, the clip range. Moreover, it was found empirically that the optimum value of γ is 0.3, and the value of clip range was increased, to a greater or lesser extent, from its default value 0.2. For instance, with this hyperparameter tuning and using Neurofoil, an agent can be trained on 60000 steps that has the same performance as one trained on 120000 steps using the default hyperparameters given by Stable Baselines 3. Figure 7 shows the mean reward that the agent obtained during training for different values of γ . As can be observed, the line for $\gamma = 0.3$ grows faster than the line for $\gamma = 0.99$, which means that the agent trained with $\gamma = 0.3$ is learning with fewer steps.

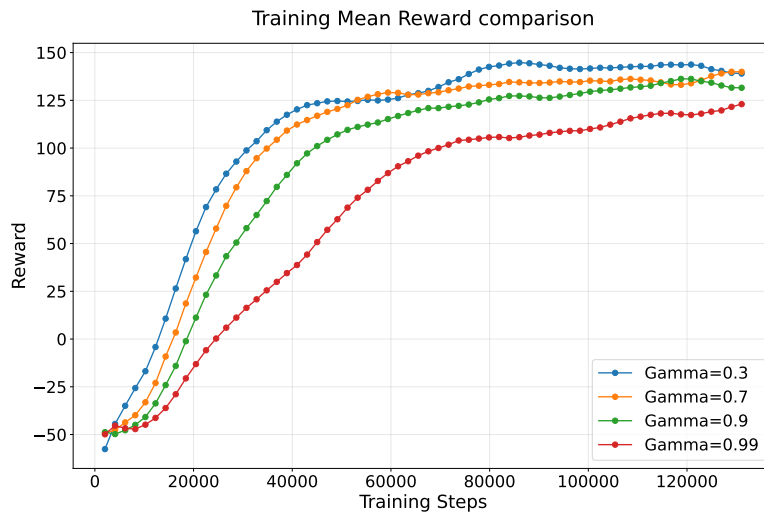


Figure 7: Episode mean reward during training with different discount factors (γ)

B.2 For agent trained with XFoil

Parameter	Value
Total timesteps	-
Learning rate	2.5×10^{-4}
Steps per update	2048
Batch size	64
Num. epochs	20
Discount factor (γ)	0.3
Clip range	0.3
Entropy coefficient	0.001
Policy net architecture	[256, 256]
Value net architecture	[256, 256]

Table 8: PPO hyperparameters for XFoil. The number of timesteps depend on the agent and will be define on its corresponding section

B.3 Fine-tuning Neuralfoil and XFoil

Parameter	Value
Total timesteps	26312
Learning rate	2.5×10^{-4}
Steps per update	2048
Batch size	64
Num. epochs	10
Discount factor (γ)	0.3
Clip range	0.6
Entropy coefficient	0
Policy net architecture	[256, 256]
Value net architecture	[256, 256]

Table 9: PPO hyperparameters of the pretrained Neuralfoil agent

Parameter	Value
Total timesteps	10240
Learning rate	2.5×10^{-4}
Steps per update	512
Batch size	64
Num. epochs	20
Discount factor (γ)	0.3
Clip range	0.2
Entropy coefficient	0.005
Policy net architecture	[256, 256]
Value net architecture	[256, 256]

Table 10: PPO hyperparameters of fine tuning XFoil agent

C XFoil configuration

Parameter	Value
Maximum Iterations	200
Number of Panels	255
Critical Amplification Factor (n_{crit})	9
Timeout	30 seconds
Angle of Attack (α)	2°
Reynolds Number (Re)	1×10^6
Mach Number (Ma)	0.5

Table 11: XFOIL configuration